MPC-Based Haptic Shared Steering System: A Driver Modeling Approach for Symbiotic Driving

Andrea Michelle Rios Lazcano ⓘ, Tenghao Niu, Xabier Carrera Akutain, David Cole ⓘ, and Barys Shyrokau ⓘ

Abstract—**Advanced driver assistance systems (ADAS) aim to increase safety and reduce mental workload. However, the gap in the understanding of the closed-loop driver–vehicle interaction often leads to reduced user acceptance. In this article, an optimal torque control law is calculated online in the model predictive control (MPC) framework to guarantee continuous guidance during the steering task. The research contribution is in the integration of an extensive prediction model covering cognitive behavior, neuromuscular dynamics, and the vehicle-steering dynamics, within the MPC-based haptic controller to enhance collaboration. The driver model is composed of a preview cognitive strategy based on a linear-quadratic-gaussian, sensory organs, and neuromuscular dynamics, including muscle coactivation and reflex action. Moreover, an adaptive cost-function algorithm enables dynamic allocation of the control authority. Experiments were performed in a fixed-base driving simulator at Toyota Motor Europe involving 19 participants to evaluate the proposed controller with two different cost functions against a commercial lane keeping assist system as an industry benchmark. The results demonstrate the proposed controller fosters symbiotic driving and reduces driver–vehicle conflicts with respect to a state-of-the-art commercial system, both subjectively and objectively, while still improving the path-tracking performance. Summarising, this article tackles the need to blend human and ADAS control, demonstrating the validity of the proposed strategy.**

Index Terms—**Collaborative driving, driver modeling, haptic shared control (HSC), human–machine interaction, model predictive control (MPC).**

I. INTRODUCTION

THE exponential growth of advanced driver assistance systems (ADAS) over the years has a direct impact on increased safety and reduction of mental workload while driving [1]. However, automation can also lead to unsatisfactory user acceptance when the driver's intention or expectation does not match the behavior of the driving assist system [2].

Moreover, the different projections toward the deployment of fully automated vehicles (AV) predict several decades of progressive increase of automation before self-driving cars become widespread [3]. Vehicles with partial level of automation provide intermediate scenarios, from basic driving aids to effective shared control between human and artificial intelligence (AI).

The shared control approach is particularly suitable for the steering task as forces can be exchanged at the steering wheel to accomplish a common objective. Through haptic shared control (HSC), the authority of the driving task is balanced between the driving assist system and the driver. However, although HSC can lead to less steering control activity and increased safety [4], drivers sometimes resist the assist system's guidance [5]. This can be due to, for example, a mismatch between the driver's cognitive intentions and the controller's objective, or, from a neuromuscular level, the reflex action of the muscle spindles [6].

Therefore, the closed-loop driver–vehicle interaction needs to be carefully reviewed in order to design collaborative, user-accepted systems. On the one hand, there is an increasing interest in the study of driver models applicable to the driving task. However, human complexity and unpredictability have made it difficult to guarantee collaboration and seamless control. On the other hand, the difficulty to find objective metrics to analyze these closed-loop dynamics incentivises the use of driver models in the development of new driving assist systems to be able to determine, which characteristics are the cause of certain subjective feelings. In the literature, the need to blend driver modeling and vehicle control systems has been widely acknowledged [7], [8], but there has been limited implementation of detailed driver models in haptic shared controllers [9]. An in-depth literature review of shared control for AVs [10] presents an overview of all model-based HSC algorithms tested with drivers in-the-loop, and discusses the positive impact that including a driver model has in the reductions of conflicts is highlighted.

In particular for the steering task, some research studies have tried to consider the driver–vehicle interaction, in which the MPC strategy is often recognised as the most attractive control

approach. However, oversimplified models, representing the arms as a simple spring damper system, have been commonly used. In a lane-keeping assist [11], this interaction is modeled by coupling the arm dynamics to the steering system, and this was also extended to a lane-changing scenario [12], using MPC. Together with a simple arm model, an attempt to introduce an adaptive level of control authority within the MPC cost function is presented in [13], but the results were constrained to a constant level of control authority for the shared driving case. In [14], an adaptive level of control authority is exploited to improve takeover requests from automation to driver, which further demonstrates the importance of appropriately balancing the authority in shared control. A more extensive psycho-physiology-based driver model is implemented in [15] for an LKA case; however, there was only one participant in the experiment. In addition, the creation of important key performance indicators (KPIs) to assess the collaborative behavior of the assistance is remarkable. From a more theoretical approach, the use of game theory models in [16]–[18] have also been designed using MPC to capture the driver-ADAS interaction. Furthermore, the model developed in [19] takes special care in tackling the human–machine conflicts, but the human-compatible reference used by the haptic shared controller is calculated offline. Thus, no modification during online simulations is possible. Finally, from the results of these studies, it can generally be seen that the conflicts in torque between driver and driving assist system are not successfully addressed and drivers either fight or correct the torque guidance instead of collaborating with it.

This article presents a case of HSC to provide continuous guidance during the steering task, in which the optimal torque control law is calculated in the model predictive control framework. The novel contribution of the proposed study is the predictive controller including the enhanced driver model (cognitive behavior and neuromuscular dynamics) and the vehicle-steering dynamics. Such an approach helps us to foster collaboration between the assist controller and human-being providing a more pleasant driving experience compared to the conventional ADAS.

The rest of this article is organized as follows. Section II establishes the steering-vehicle dynamics. Section III describes the theory behind the driver model integrated within the MPC system, and Section IV presents the results of its validation in a driving simulator pilot experiment. Afterward, in Section V, the MPC strategy is introduced. Section VI includes the details of the subsequent driving simulator experiments to evaluate the proposed driving assist system. In Section VII, the objective and subjective results of a benchmark comparison between a commercial LKA and two different collaborative modes of the proposed MPC controller can be found. Finally, Section VIII, concludes this article.

II. STEERING-VEHICLE MODEL

A. Vehicle Dynamics

The vehicle dynamics presented in Fig. 1 are based on the linear single-track model. The model assumes a constant longitudinal velocity, linear tyre dynamics, and small angle approximations. This model simplification can capture the vehicle
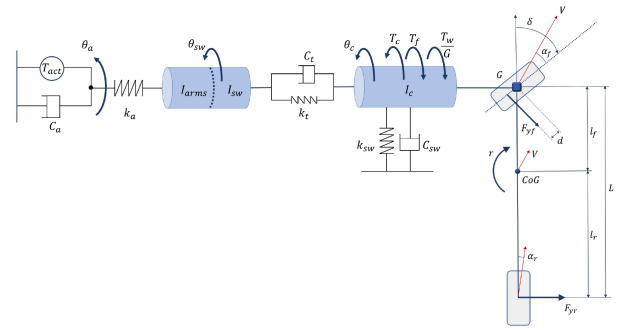

Fig. 1.　Arms-steering-vehicle model.

handling characteristics within the scope of this investigation. Particularly, a range of lateral acceleration up to 4 m/s^2 for passenger cars, which includes path-following tasks in nonevasive manoeuvres. Moreover, the selected steering-vehicle parameters are derived from the complete nonlinear steering-vehicle plant to ensure its applicability for standard manoeuvres at 100 km/h.

Equations (1) and (2) represent the linearized vehicle motion where m is the vehicle mass and I_{zz} is the inertia with respect to the centre of mass. The vehicle front and rear distance from the centre of gravity are denoted by l_f and l_r, respectively. Moreover, the states of the vehicle are longitudinal V_x and lateral V_y, vehicle velocities, yaw rate r, and heading angle ψ

$$m(\dot{V}_y + V_x r) = F_{y,f} + F_{y,r} \tag{1}$$

$$I_{zz}\ddot{\psi} = l_f F_{y,f} - l_r F_{y,r}. \tag{2}$$

The lateral axle forces $F_{y,i}$ have a linear relation with respect to the slip angles α_i with $i \in \{f, r\}$ to represent the front and rear axle, and are calculated as

$$\alpha_f = -\delta + \frac{V_y + l_f r}{V_x} \tag{3}$$

$$\alpha_r = \frac{V_y - l_r r}{V_x} \tag{4}$$

$$F_{y,f} = -C_{\alpha_f,f}\alpha_f \tag{5}$$

$$F_{y,r} = -C_{\alpha_r,r}\alpha_r. \tag{6}$$

B. Steering System Dynamics

The introduction of the steering system dynamics is key to investigate the interaction between driver and driving assist system. The steering dynamics are rigidly coupled to the arms dynamics at the steering wheel, where torques are exchanged. Thereby resulting in a lumped inertia that is the sum of the inertia of the arms I_{arms} and the inertia of the steering wheel I_{sw}. The neuromuscular dynamics of the arms are described in detail in Section III-B.

The linear steering dynamics [20] are represented in (7) and (8) with 2-degrees-of-freedom (DoF), where the steering wheel angle θ_{sw}, and steering column angle θ_c denote each DoF. The interaction of the driver is taken into account through the introduction of the muscle angle of the arms θ_a, which also interacts with the steering wheel. The difference of the angles at the steering column is defined as $\Delta\theta_{sc} = (\theta_{sw} - \theta_c)$, and the
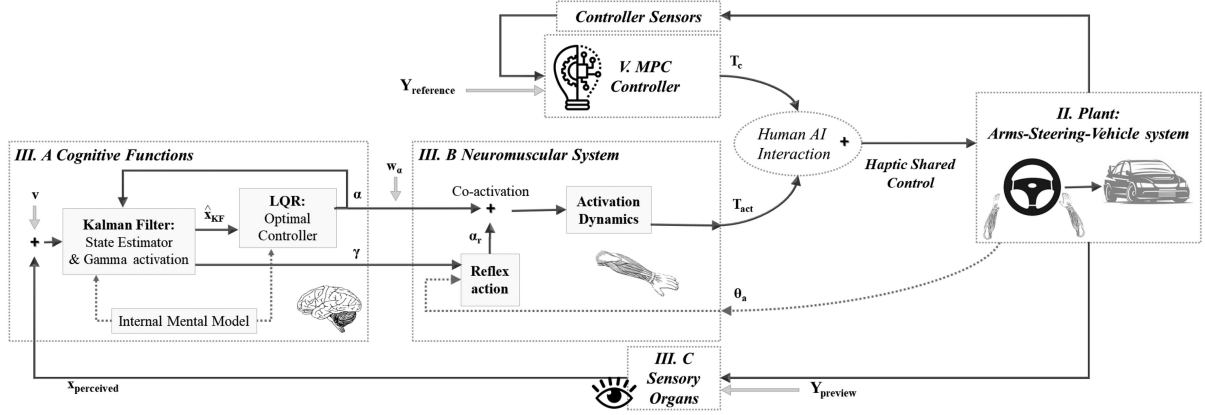
Fig. 2.   HSC scheme with driver model representation. A detailed description of each block can be found in the corresponding sections.

same notation follows for their derivatives with respect to time, $\Delta\dot\theta_{sc} = (\dot\theta_{sw} - \dot\theta_c)$

$$(I_{sw} + I_{arms})\ddot\theta_{sw} = k_a(\theta_a - \theta_{sw}) - c_t\Delta\dot\theta_{sc} - k_t\Delta\theta_{sc} \tag{7}$$

$$I_c\ddot\theta_c + c_{sw}\dot\theta_c + k_{sw}\theta_c = c_t\Delta\dot\theta_{sc} + k_t\Delta\theta_{sc} - \frac{T_w}{G} - T_f + T_c \tag{8}$$

where I_c denotes the inertia of the rack and the front wheels with respect to the pinion, k_t and c_t are the steering column stiffness and the torsion bar damping, respectively, and c_{sw} and k_{sw} are the damping and self-centering stiffness with respect to the steering wheel axle.

Moreover, the road wheel angle is calculated proportionally to the steering angle column with the steering gear ratio G

$$\delta = \frac{\theta_c}{G}. \tag{9}$$

The torques interacting at the steering wheel consist of the self-aligning moment T_w, the friction moment T_f, and the torque input from the driving assist system, T_c, calculated through the MPC strategy described in Section V. The torque generated about the king-pin axes is

$$T_w = F_{y,f}d \tag{10}$$

where d is the pneumatic trail.

III. DRIVER MODEL

The integration of a realistic driver model is central to the design of the collaborative shared control strategy. A better accuracy of the torque predictions can directly improve the collaborative behavior of the proposed driving assist system.

The driver model, as presented in Fig. 2, was developed by Niu and Cole [20], building upon earlier work by Nash and Cole [21]. The model is implemented in Simulink and the cognitive model is adapted to enhance its validity in realistic scenarios with real-time capability. It aims to represent the cognitive and physiological mechanisms of the human driver, and includes an internal model, neuromuscular dynamics, sensory dynamics,

sensorimotor noise, state estimation, and cognitive and reflex control. In particular, the inclusion of neuromuscular dynamics makes the model appropriate for the development of a new driving assist system with torque feedback.

A. Cognitive Behavior

The cognitive model is used to predict the driver's steering intentions. For the cognitive control, a predictive approach is based on a linear-quadratic regulator (LQR). Moreover, the states of the system are estimated with a Kalman filter to reduce the effect of measurement noise of the sensory organs and process noise of the muscle activation. This combination of approaches is also known as the linear-quadratic-Gaussian and it requires an accurate internal mental representation of the plant in order to achieve optimal state estimation. In this regard, a forward internal mental model is assumed to be acquired *a priori* by the driver.

The cost function of the LQR, which calculates the expected driver torque input, is adapted and modified based on previous work [21], [22]. This function minimizes the lateral deviation of the vehicle with respect to the upcoming reference trajectory of the road with a certain preview time T_{prev}

$$J_{LQR} = \sum_0^\infty \left[\begin{bmatrix} \mathbf{x}_{KF} & \mathbf{y}_p \end{bmatrix} \mathbf{C}^T\mathbf{Q}\mathbf{C} \begin{bmatrix} \mathbf{x}_{KF} \\ \mathbf{y}_p \end{bmatrix} \right] + \alpha R\alpha \tag{11}$$

where $\mathbf{C}$ is a matrix that selects the states on the lateral position, heading angle, and the road preview points. Finally, the expected driver torque input, α, is calculated as

$$\alpha = -\mathbf{K}_{LQR} \begin{bmatrix} \mathbf{x}_{KF} \\ \mathbf{y}_p \end{bmatrix} \tag{12}$$

where $\mathbf{K}_{LQR}$ is the LQR gain, $\mathbf{x}_{KF}$ is a 20x1 vector with the estimated states as derived from [20], and $\mathbf{y}_p$ is a vector containing the upcoming preview lateral road coordinates of length $N_p = T_{prev}/T_{s,DM}$. The estimated states include the lateral reference target path, the arms-steering-vehicle states, the muscle activation states, and the delayed states perceived through the

TABLE I
DRIVER MODEL PARAMETERS

Parameter	Value	Parameter	Value
T_{prev}	1.4 s	I_{arms}	0.0718 kg m^2
k_a	30 Nmrad	c_a	3 Nms/rad
k_r	21 Nm/rad	τ_r	0.04 s
τ_1	0.03 s	τ_2	0.02 s
τ_{visual}	0.24 s	τ_{muscle}	0.19 s
Q	diag($3 \cdot 10^3$, $1 \cdot 10^2$)	R	1

sensory organs. The rest of the cost function parameters can be found in Table I.

B. Neuromuscular Dynamics

The muscle dynamics are described by a linearized Hill-muscle model [23]. The elasticity of the tendons is represented by the stiffness term, k_a. The contractile element, on the other hand, is described by the damping term, c_a, and the neural activation torque T_{act}, which is a function of the desired driver torque and the reflex action.

The neuromuscular dynamics of the driver are, thus, composed of the reflex action of the muscle spindles, a linearized Hill-muscle model including the activation dynamics of the muscles, and the muscle dynamics of the arms, which are interacting with the steering system. These elements are necessary for the modeling of the coactivation mechanism of the muscles

$$T_{act} = c_a \dot{\theta}_a + k_a(\theta_a - \theta_{sw}). \tag{13}$$

The activation dynamics, denoted by H_{act}, are subject to a lag time constant of the motor neurons excitation, τ_1, and a lumped neuro-muscular transduction delay, τ_2. The latter time constant represents the muscle activation and deactivation lag

$$H_{act} = \frac{1}{(\tau_1 s + 1)(\tau_2 s + 1)}. \tag{14}$$

The reflex loop, an essential element of the coactivation mechanism, is subject to a delay time constant, τ_r, and a gain factor, k_r. The expected muscle angle, γ, is calculated based on the internal mental model of the driver and the estimated states by the Kalman filter

$$\alpha_r = \frac{k_r}{\tau_r s + 1}(\gamma - \theta_a). \tag{15}$$

C. Sensory Organs

The sensory organs modeled are the visual perception organs, and the proprioceptors with the purpose of representing the human limitations in the perception. The modeling of the vestibular organs is considered out of the scope of this research because the validation is carried out in a fixed-base driving simulator [24]. The states perceived by the driver are the vehicle lateral deviation with respect to the desired path, e_y, the heading angle ψ, and the muscle angle of the driver θ_a. These states are subject to a visual delay τ_{visual} and a muscle sensory delay τ_{muscle}. The feedback sensed by these organs is then sent to the central nervous system, subject to additive measurement noise. These noisy signals are used to estimate the states of the plant with the
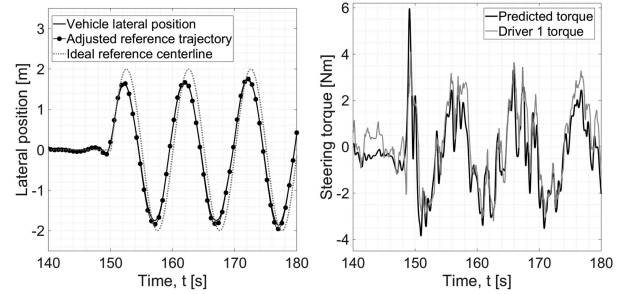

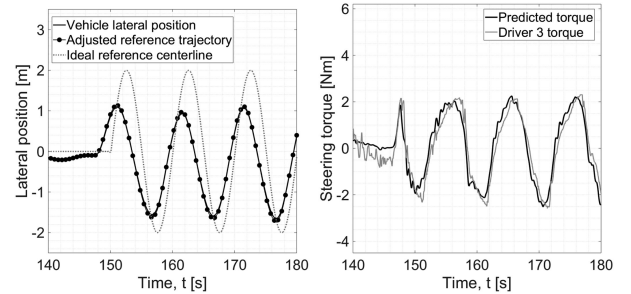Fig. 3.   Driver model predictions based on driver 1, novice.

Fig. 4.   Driver model predictions based on driver 3, expert level.

TABLE II
TORQUE PREDICTION ACCURACY OF THE DRIVER MODEL

Driver	RMSE [Nm]	% Accuracy
Driver 1: Novice	0.7344	89.96
Driver 2: Intermediate	0.6232	90.96
Driver 3: Expert	0.7355	87.30

Kalman filter model, based on the assumption that the driver has a good internal mental representation of the vehicle and their own neuromuscular dynamics. In future work, the introduction of signal-dependent noise, as presented in [25], is of high interest. The parameters of the driver model are listed in Table I. Most values are extracted from [20], whereas T_{prev} and Q are selected based on the pilot experiment, described in Section IV.

IV. DRIVER MODEL VALIDATION

As a first step in the validation of the driver model, the predictions of the torque are simulated offline in IPG CarMaker. Here, the driver model is compared to the IPG CarMaker virtual driver. To represent the plant, we use nonlinear vehicle dynamics and a proprietary nonlinear steering system [26] with a Toyota production vehicle parametrization. This allows for a high-fidelity simulation of real-world scenarios. Afterward, a driver-in-the-loop pilot experiment was performed.

A. Pilot Experiments With Driving Simulator

A pilot study was performed at Toyota Motor Europe, using the fixed-base driving simulator of Fig. 6. Three different drivers, listed in Table II in ascending order of driving experience, participated in the experiment to further validate the accuracy of the driver model. In order to test the driver model performance
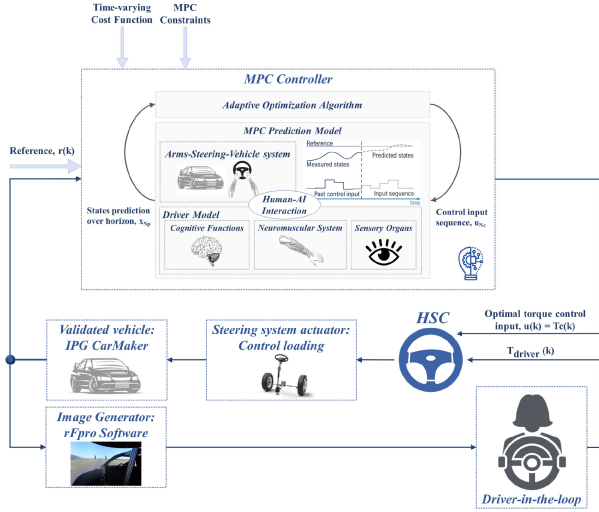
Fig. 5.   Set-up for the driving simulator experiment at Toyota Motor Europe, Belgium.

Fig. 6.   Driving simulator at Toyota Motor Europe, Belgium.

for different driving styles and behavior, there is significant variability in the drivers' experience. Namely, the participants are a novice driver, a driver with 12-years of experience, and a driver with over 20 years of driving experience and expert knowledge in driving simulators.

B. Results and Discussion

The driver model fits all three drivers well, as objectively shown in Table II, which further demonstrates the capabilities of the model to capture inter- and intradriver variability.

The driver model parameterization is found to match slightly better the novice and intermediate driver, which could be because the linear internal mental model captures better users with limited driving experience, whereas the mismatch between the linear model and the knowledge of expert drivers is more significant.

The sensitivity of the different driver model parameters was studied preliminarily in order to obtain the best possible fit. From this analysis, the driver preview time of the road is highlighted and was tuned for each driver. This can be linked to the different cognitive strategies that each driver has in order to follow the road path. The novice driver, in Fig. 3, tends to have a shorter preview time, as well as a noisier torque input. On the other hand, for the most experienced driver, in Fig. 4, even though the perception of the ideal road trajectory was not correct, the torque input is smooth. This can be associated with the accuracy of internal knowledge that the experienced driver has concerning

the vehicle dynamics, which influences the level of muscle spindles activation.

Another relevant factor is that having the correct human road preview is key for the model to give an accurate torque prediction. A good fitting of the prediction was obtained for the three drivers under the assumption that the vehicle position corresponds to the desired vehicle trajectory. This assumption would not be valid in the presence of, for instance, external disturbances, in which case the muscle spindles torque would be activated.

V. MPC FRAMEWORK

In this section, an overview of the mathematical background of the proposed MPC-based LKA controller is presented. The general goal of the MPC is to iteratively calculate the trajectory of a future control input, $u(k)$, to optimize the performance of the plant being controlled by minimizing a cost function subject to constraints. The optimization takes into account the plant states' information, $x(k)$, at the start of the time window. The length of this finite-time window is called the prediction horizon, N_p. The control horizon of the control input sequence is set equal to the prediction horizon.

The MPC approach can compute the optimization online and in real-time integrating the driver's torque control behavior in the loop, thereby capturing the haptic interaction.

A. Structure of the MPC

The need for accurate precision in the steering task makes the MPC technique highly attractive for the development of ADAS systems. In this framework, we can introduce constraints on the control inputs and the states of the plant to guarantee safety, smooth control, and driving comfort.

The general structure of the prediction model is

$$\mathbf{x}(k+1) = f(\mathbf{x}(k), u(k)), \text{ with } \mathbf{x}(0) = \mathbf{x}_0 \qquad (16)$$

where $\mathbf{x}$ is the vector of the system states, with $\mathbf{x} \in \mathbb{R}^{38}$. The variable $\mathbf{x}_0$ denotes the initial states, and f is the function describing the equations of the prediction model. Lastly, the variable $u \in \mathbb{R}^{N_u}$ is the control input, with $N_u = 1$ in this article.

The complete vector of states is

$$\mathbf{x}(k) = [y \ V_y \ \psi \ r \ \theta_{\text{sw}} \ \dot{\theta}_{\text{sw}} \ \theta_{\text{sc}} \ \dot{\theta}_{\text{sc}} \ \dots$$
$$\theta_a \ x_{H\text{act}} \ T_{\text{act}} \ e_{yd} \ \psi_d \ \theta_{ad} \ \dots$$
$$\mathbf{x}_{\text{KF}} \ \gamma \ \alpha_r \ \alpha \ T_c]^T. \qquad (17)$$

And the control input is the torque control rate $\dot{T}_c$.

B. Cost Function and System Constraints

The constraints are essential to consider the driver–vehicle limitations, as well as guaranteeing smooth control inputs to enhance driving comfort.

The cost function of this MPC-based haptic steering controller in (18) improves the path-tracking performance and reduces the driver–vehicle conflicts. Moreover, the settings are tuned

TABLE III
MPC SETTINGS AND WEIGHTS

Variable	Value	Variable	Value
$T_{s,mpc}$	$1 \cdot 10^{-2}$ s	$T_{s,sim}$	$1 \cdot 10^{-3}$ s
N_p	40	W_y	$1 \cdot 10^6$
W_{y_N}	$1 \cdot 10^2$	W_ψ	$V_x \cdot W_y$
W_{T_c}	600	$W_{T_{input}}$	40
W_{V_y}	$1 \cdot 10^2$	W_r	$1 \cdot 10^2$
$W_{spindles}$	$1 \cdot 10^2$	W_{driver}	$6 \cdot 10^2$
$|V_{y,max}|$	4 m/s	$|r_{max}|$	50 deg/s
$|\theta_{sw,max}|$	360 deg	$|\dot{\theta}_{sw,max}|$	800 deg
$|T_{c,max}|$	10 Nm	$|\dot{T}_{c,max}|$	20 Nm/s

to allow the assist system to provide a more intuitive torque guidance to the driver through the steering interface

$$J(\mathbf{x}, u) = \sum_{k=0}^{N_p-1} \|(\mathbf{x}_k - \mathbf{y}_{r,k})\|_{\mathbf{W}_x}^2 + \|u_k - u_{r,k}\|_{W_u}^2$$
$$+ \|\mathbf{x}_{N_p} - \mathbf{y}_{r,N_p}\|_{\mathbf{W}_{x_N}}^2 \qquad (18)$$

where $\mathbf{W}_x$, $\mathbf{W}_{x_N} \geq 0$ are the weighting matrices of the stage and terminal cost for the states. The parameter $W_u > 0$ corresponds to the stage cost for the input. The time-varying state reference vector is denoted as $\mathbf{y}_r$ and input reference $\mathbf{u}_r$.

The selected costs for the MPC system can be seen in Table III. First of all, the tracking performance objective is implemented to minimize the lateral deviation with respect to the reference path, subject to a look-ahead distance factor depending on the vehicle velocity and the heading angle ψ. Moreover, driving comfort can be enhanced through weights on the lateral velocity V_y and the yaw rate r. Additional costs on the driver's effort or discomfort indicators can also be added to reduce the activation of the muscle spindles' torque or the total driver steering torque.

Furthermore, the MPC model is subject to constraints, defined in Table III in absolute maximum value. These constraints are imposed on the lateral velocity and the yaw rate. Moreover, constraints on the steering wheel angle θ_{sw} and assist torque input T_c as well as their respective rates are also introduced to guarantee a smooth assist guidance. Hard constraints on the driver model states are avoided for stability and, instead, weights to penalise their magnitude are included.

The different sampling times and prediction horizons, as specified in Table III, are appropriately chosen to ensure that the controller can be run in real-time without compromising its performance, prediction capabilities, and stability. The nonlinear plant operates at a higher sampling frequency, $T_{s,sim}$, whereas the linear driver model can be accurately run at a lower sampling frequency, $T_{s,DM}$, which reduces the computational requirements. For the MPC, the maximum sampling frequency that allows the model to compute the optimal control input in real time, $T_{s,mpc}$, is selected to ensure stability and a long enough prediction time, $T_{s,mpc} \cdot N_p$, which has a direct impact on its performance.

C. Adaptive MPC for Conflict Minimization

Human behavior is adaptive and time-varying. Therefore, one approach to deal with the competing behavior between human

and driving assist systems is to adapt the level of automation [27]. However, due to the increased complexity of the dynamic task allocation, most research studies implement binary switches of control authority.

In this research, the MPC optimization problem is solved with the ACADO Toolbox [28]. This software allows us to implement an adaptive cost function algorithm through time-varying weights. These dynamic characteristics aim to minimize conflicts between the applied driver torque and the driving assist system torque, as well as dynamically share the control authority. Adaptive weights are applied to the MPC controller torque and its rate based on the online difference with the driver torque. This feature further enhances collaboration. For instance, an increase in the control input torque cost results in higher driver control authority. On the other hand, if there are no torque conflicts, the cost is smoothly reduced, which results in less driver steering effort and a higher level of control authority for the collaborative automation system.

The trigger for the adaptive weights is the presence of torque conflicts between driver and assist system, represented by a step signal. In order to ensure smooth transitions, this step signal is converted to a parabolic shape p by applying a moving average filter, MAV, and the following operations:

$$x = \left[1 - \frac{\text{MAV} - W_{Tc}}{b_T W_{Tc} - W_{Tc}} 2 \right] \qquad (19)$$
$$p = 1 - 0.0067x - 0.7x^2 + 0.2267x^3 \qquad (20)$$

with p in the range of $[0, 1]$. This is then scaled to $[W_{Tc}, b_T W_{Tc}]$ and $[W_{Tinput}, b_{Tr} W_{Tinput}]$ for the costs of the controller torque and torque rate input, respectively. The increase factors are $b_T = 2$ and $b_{Tr} = 1.5$.

This adaptive cost has fast increments to better tackle conflicts and slow reductions, reaching the minimum cost value in a longer time frame. The velocity of the cost transition is determined with size of the moving average filter window.

VI. DRIVING SIMULATOR EXPERIMENT: COLLABORATIVE LANE KEEPING ASSIST

The aim is to assess the performance and collaborative behavior of the proposed MPC controller with two different cost-function settings, as well as to compare them against a commercial LKA used as a benchmark. All three controllers provide the drivers with haptic torque guidance to track the centre of the path.

A. Driving Scenario

The driving scenario designed was a route of 5 km long with four straight segments and four sinusoidal segments of different amplitudes. In every trial, the vehicle was driving at a constant vehicle speed of 100 km/h and the test subject's sole task was to control the lateral motion of the vehicle to drive in the centre of the lane. In order to allow for more driver variability, the lane width was set to 5 m and no lane markings were present. The importance of this variability is to better assess how the different LKA systems react and adapt to driver behaviors and diverse

driving strategies. This is fundamental to obtain a meaningful comparison of the collaborative behavior of the different assist systems proposed. An overview of the set-up for this driver-in-the-loop experiment can be seen in Fig. 5, where the drivers interact with the controller through the steering torque feedback. The graphics were rendered with rFpro software based on an IPG CarMaker scenario in a 210^0 projection screen, which can be seen in Fig. 6.

B. Experimental Procedure

The experimental procedure was the same for all 19 participants, with drivers ranging from 22 to 41 years old. All participants are engineers at Toyota with comprehensive knowledge on vehicle dynamics, with an average age of 29.7 years (SD = 6.9) and 10.7 years (SD = 8.0) of driving experience. A relevant note is that three of the drivers have extensive professional experience assessing LKA systems. The experiment consisted of independent trials for each of the three driving assist systems evaluated. During each trial, the driving scenario and the task were the same and the drivers were not informed of which assist system they were using at any point. The consistency and statistical significance of the results strengthens the expectations that the number of participants was sufficient for this article.

At the start of the experiment, the participants were instructed of the task and the experimental conditions. The order of the trials was randomized to avoid human bias. During the experiment, the first minute of each trial was used as training. This initial data are discarded from the objective metrics and its purpose is to allow drivers to familiarize themselves with the assist system and the driving simulator.

C. Lane Keeping Assist Controllers

The controllers assessed during this experiment are described as follows.

1) Baseline Lane Keeping Assist: The MPC modes are evaluated against a commercial LKA system, described in Appendix A. The current systems available in the automotive industry are mainly focused on minimizing a lateral offset and they do not integrate the driver interaction nor their impact on the closed-loop dynamics. This approach aims to improve the path-tracking performance, but it can result in a torque guidance with suboptimal acceptance.

2) MPC Mode 1: The MPC framework makes it possible to change the behavior of the controller through different cost-function parameterizations. The first MPC mode, which corresponds to a typical cost-function algorithm, has weights on the lateral error, yaw angle, and other vehicle states, as defined in Section V. The costs on the driver model states are set to zero in this cost-function. However, the driver behavior is taken into account by having the extensive driver model from Section III within the prediction model of the controller, aiming for a more human intuitive guidance.

3) MPC Mode 2: The second MPC parameterization makes explicit use of the driver model in the cost-function through the introduction of additional weights on the driver torque and muscle spindles torque predicted by the driver model, which can
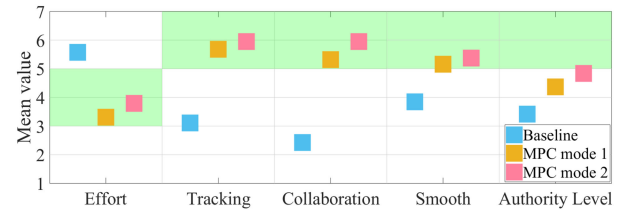

Fig. 7. Mean results of the subjective evaluation of 19 participants.

be found in Table III. Specifically, the proposed MPC controller tries to minimize the muscle spindles activation, which is related to the rejection of disturbances and muscle discomfort at a neuromuscular level. Moreover, the adaptive behavior of the MPC is further customized to reduce conflicts with the driver. For this purpose, the cost when the driving assist torque is opposing the real driver, as described in Section V-C, is increased.

VII. RESULTS AND DISCUSSION

Statistical significance of the metrics was verified using a one-way ANOVA test comparing the three different LKA systems. First of all, to ensure the robustness of the results, a Bartlett's test for equal variances between the three groups of controllers was executed. In the subjective evaluations, the null hypothesis of equal variances is rejected for the second criteria (tracking performance), thus, a nonparametric Kruskal–Wallis test was performed in this case. A similar approach is applied to the objective metrics.

A. Subjective Evaluation

A questionnaire based on a seven-point scale with a total of five questions was designed to subjectively assess the behavior of each LKA. At the end of the experiment, the participants were also asked to rank the three systems from best to worst. The outcomes of these evaluations show that the proposed MPC controllers outperform the baseline benchmark, with 84.21% of the subjective responses choosing the MPC mode 2 as the best LKA system, and the remaining 15.79% choosing MPC mode 1. The assessed characteristics are listed as follows:

1) Overall Steering Effort: Based on the torque applied by the driver, with the ideal range between 3 and 5 points.
2) Performance and Guidance Level: Defined in terms of the path-tracking performance of the ideal centerline. A range of 6–7 corresponds to high tracking precision.
3) Collaborative Behavior: An evaluation of 6–7 points means that torque conflicts between the driver and driving assist system are reduced.
4) Feeling of Being in Control: Defined in terms of how easily the drivers feel that they can overrule the assist guidance if desired, with 6–7 points if it is easy.
5) Smooth Control: In terms of the presence of unnecessary corrections during authority transitions between the driver and assist system control. The lower range being abrupt (1–2) and the upper range smooth (6–7) control.

Fig. 7 presents the average grade of each subjective metric per controller. The ideal range is highlighted in light green. This is

TABLE IV
ANALYZED DATA OF THE SUBJECTIVE EVALUATIONS

Criteria	Baseline	MPC 1	MPC 2	F	p
Overall effort	5.58 (0.90)	3.32 (1.25)	3.79 (1.18)	21.53	<0.001
Tracking performance	3.11 (1.73)	5.68 (1.11)	5.95 (0.91)	27.86	<0.001
Collaborative behaviour	2.42 (1.35)	5.32 (1.00)	5.95 (1.08)	50.60	<0.001
Feeling of control	3.42 (1.74)	4.37 (1.34)	4.84 (1.50)	4.21	0.02
Smooth control	3.84 (1.34)	5.16 (1.57)	5.37 (1.67)	5.51	0.007

TABLE V
ANALYZED DATA OF THE OBJECTIVE METRICS

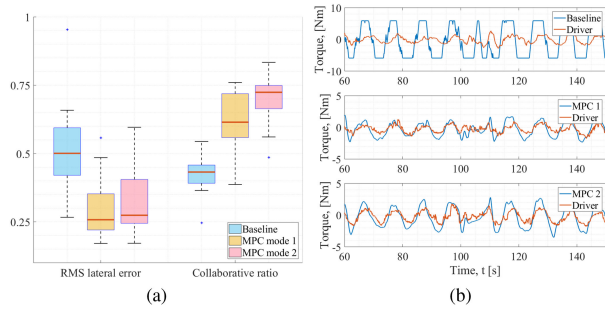| Criteria	Baseline	MPC 1	MPC 2	F	p
Driver effort	177.01 (37.74)	51.32 (37.38)	78.83 (50.31)	46.49	< 0.001
Controller effort	2982.77 (170.05)	209.83 (92.90)	390.08 (193.23)	43.17	<0.001
Lateral RMSE	0.51 (0.15)	0.29 (0.11)	0.33 (0.12)	15.38	<0.001
Maximum e_y	1.14 (0.54)	0.66 (0.33)	0.75 (0.43)	6.17	0.004
Mean e_y	-0.06 (0.19)	0.03 (0.15)	0.03 (0.18)	1.81	0.173
SD e_y	0.47 (0.16)	0.25 (0.10)	0.28 (0.10)	17.53	<0.001
Collaborative ratio	0.43 (0.06)	0.62 (0.11)	0.70 (0.09)	45.70	<0.001
Intrusiveness ratio	0.57 (0.06)	0.38 (0.11)	0.30 (0.09)	45.70	<0.001
Resistance ratio	0.28 (0.04)	0.20 (0.13)	0.16 (0.11)	16.10	<0.001
Contradiction ratio	0.29 (0.04)	0.18 (0.13)	0.14 (0.11)	18.50	<0.001
Coherence	-0.17 (0.17)	0.15 (0.29)	0.36 (0.27)	21.88	<0.001
Level of control authority	17.56 (3.68)	7.73 (8.03)	8.22 (8.79)	20.91	<0.001
Steering reversal rate	31.84 (12.84)	23.76 (5.27)	22.68 (6.75)	8.38	0.015

Fig. 8.   (a) Box plot of the objective KPIs of 19 participants. (b) Torques over time for participant 1.

consistent with the preference of drivers to use the second mode of the proposed MPC.

The participants consistently felt that proposed MPC controllers provide an even more natural feel than the state-of-the-art baseline system. In general, the presence of driver–assist conflicts creates a perception of the baseline controller being heavier than desired, as well as having a lower collaborative behavior. Moreover, drivers do not perceive small path-tracking errors that the baseline assist tries to minimize, which may explain a higher degree of conflict and, eventually, decreased the tracking performance. The feeling of being in control, as expected, is lower because part of the control authority is shared with the assist system. However, the MPC modes are still graded higher than the baseline system for this last subjective quality, as well as providing an even more smooth guidance.

Statistical significance of the responses was positively verified, which can be seen in Table IV. For all five subjective metrics, MPC mode 2 is the best, closely followed by the fist MPC mode. The mean value of the responses for each metric, as well as their standard deviation (SD) are also included.

B. Objective Assessment

The objective evaluation is based on an extensive list of KPI, which can be seen in Appendix B, based on a recompilation of both research studies and industry standard metrics. These metrics were meticulously selected to impartially evaluate the responses to the subjective questions. Fig. 8 shows the box plot of two representative objective metrics. In the following paragraphs, the values of the numerical differences between the proposed MPC mode 2 and the baseline benchmark LKA are

discussed. In Table V, the results of the one-way ANOVA test are presented, as well as the mean and SD values of each metric. From this, it is clear that the proposed MPC controllers significantly decreased the overall driver steering effort, in particular, with an average reduction of 55.47% with respect to the baseline system. This is in agreement with the subjective evaluation of the MPC modes, which were judged as lighter steering systems. The explanation lies in the behavior of the MPC controllers, which actively cooperate with the driver and minimize the conflict, as can be seen in Fig. 8. In other words, the intuitive, continuous guidance of the MPC modes makes an efficient use of the torque feedback to achieve better symbiosis with the driver. Objectively, the collaborative ratio of the MPC controller in mode 2 increases by 62.86% with respect to the baseline benchmark.

Moreover, even though the baseline controller optimizes almost solely the tracking performance, the results show that the proposed MPC mode 2 has an improvement of 35.93% in regards to the rmse of lateral error. This can be explained because the closed-loop human–vehicle interaction is considered by the MPC controller. As previously mentioned, an accurate prediction of the driver's intention reduces conflicts. On the other hand, driver–assist conflicts can result in the decreased tracking performance and user acceptance.

Furthermore, the level of control authority is assessed in terms of the ratio between the torque effort of the controller and the driver. As expected, the authority is greatly shared with the LKA, which relieves the driver partially from the steering workload. Even though in all three controllers the level of control authority is dominated by the assist system, in the case of the MPC modes,

the driver control is significantly higher than with the baseline system. This can lead to less driver opposition to regain control. Besides, from the subjective evaluations, most participants felt like they were still in full control with MPC mode 2. This further reassures the hypothesis that this novel LKA controller can provide a human-like, collaborative guidance. Hence, the assist system can make drivers feel in control while continuously guiding them to the correct path, decreasing driver workload, and significantly improving driving comfort. Lastly, the steering wheel reversal rate (SRR) is an indicator of the smoothness of both the control, as well as the driver workload. A lower SRR means that the driver requires less corrections to follow the target path. In this case, the proposed MPC mode 2 improves the smoothness of the control by 28.76% with respect to the baseline. A higher SRR in the baseline controller suggests that drivers tend to correct the guidance of the assist guidance.

VIII. CONCLUSION

The proposed control strategy tackles the need to blend driver and assist system through driver modeling in an HSC strategy. The controller is able to predict the human behavior and provides a smooth and intuitive guidance to the driver. The results show that the assist torque guidance matches the driver expectations and their perception of collaboration. In this article, a comprehensive driver model has been integrated in the MPC controller, providing accurate torque predictions when the driver target trajectory is known, as shown by the pilot experiments in Section IV. The MPC controller handles the nonlinearities and system constraints, which enhances driving comfort. At the same time, it allows a dynamic control authority sharing between drivers and assist system strengthening collaboration. The adaptability of the driving assist system is essential to positively cooperate with the time-varying human behavior during the steering task. Moreover, the controller can be tuned to portray different behaviors, while maximizing driving comfort and improving the tracking performance. It is important to highlight the value of an appropriate selection of the MPC cost-function weights. In order to ensure stability of the closed-loop system, sufficiently high weights must be placed to the controller torque and its rate. In addition, the introduction of a terminal cost for the lateral position further ensures closed-loop stability. The experimental results consistently show the proposed controller fosters symbiotic driving and reduces driver–vehicle conflicts. Moreover, it has been demonstrated that the proposed strategy significantly improves the performance of the currently available commercial system, both subjectively and objectively with extensive KPIs. On-going research activities are to perform more extensive tests in the driving simulator, for different scenarios, to evaluate a wider scope of steering tasks, including evasive manoeuvres. This will ensure the maximum performance and stability in a greater envelop of vehicle conditions. For this purpose, the current single-track vehicle model should be upgraded to a nonlinear vehicle model. In addition, the integration of nonlinear steering friction within the MPC prediction model is also under investigation. The influence of the steering torque friction plays an important role due to the mismatch between the

modeled nonlinear friction and more complex friction modeling for the 3-DoF steering wheel system. A higher degree of plant nonlinearities, and driver model suitability will be investigated in order to test the robustness of the proposed MPC. Lastly, a more realistic environment is needed to further assess the validity of this approach. For this purpose, the proposed MPC controller will be evaluated with a real-time control system on a physical test vehicle.

APPENDIX A
BASELINE SYSTEM

The commercial system calculates the target steering angle based on feedforward and feedback steering characteristics. The target feedback angle depends on the deviation of vehicle states with respect to certain target states quantities such as lane offset, lateral velocity, yaw angle, yaw rate, and steering angle. On the other hand, the target forward steering angle is based on a formula, which depends on the steering angle, vehicle velocity, yaw rate, lateral acceleration, lane offset, and road curvature.

In order to calculate the target angle when codriving, the ideal target control angle is combined with the actual steering angle based on a weighting factor in order to enhance codriving, as follows:

$$\theta_{\text{codr}} = \theta_{\text{sw}} + G_{\text{diff}}(\theta_{\text{target}} - \theta_{\text{sw}}). \qquad (21)$$

This weighting factor G_{diff} ranges between $[0.25, 1]$ inversely proportional to the driver torque. This factor reaches its minimum when the driver torque is more than $1.5\,\text{N} \cdot \text{m}$. To reach this target angle, the LKA calculates a target torque to be added to the EPS output of the steering system through a PID logic. The target commands are subject to magnitude and rate of change limits in order to ensure a smooth transition. Moreover, when the driver torque is opposing the target command with more than certain threshold ($3\,\text{N} \cdot \text{m}$), the torque assist is deactivated, thus, instantaneously set to zero. This way of tackling the torque conflicts can sometimes be perceived as unexpected by the driver.

APPENDIX B
LIST OF KPIS

A full list of all the KPIs found both in the literature and in the industry are listed as follows:

A. Overall Steering Effort

1) Driver torque steering effort during the time of the manoeuver se_{Td}

$$se_{Td} = \int_0^T \mathbf{T}_d^2 \, dt. \qquad (22)$$

2) Driving assist system torque steering effort during the time of the manoeuver se_{Tc}

$$se_{Tc} = \int_0^T \mathbf{T}_c^2 \, dt. \qquad (23)$$

B. Path-Tracking Performance

1) Root-mean-square error (RMSE) of the lateral position with respect to the ideal road centerline RMSE_y with N being the total number of data points

$$\text{RMSE}_y = \sqrt{\frac{1}{N} \sum_{i=1}^{N} \mathbf{e}_{y,i}^2}. \tag{24}$$

2) Maximum lateral position error $e_{y,\max}$

$$e_{y,\max} = \max(\mathbf{e}_y). \tag{25}$$

3) Mean of the lateral position error $\overline{e_y}$

$$\overline{e_y} = \frac{1}{N} \sum_{i=1}^{N} e_{y,i}. \tag{26}$$

4) SD of the lateral position error σ_{e_y}

$$\sigma_{e_y} = \sqrt{\frac{1}{N-1} \sum_{i=1}^{N} |e_{y,i} - \overline{e_y}|^2}. \tag{27}$$

C. Collaborative Behavior

1) Consistency ratio [15] r_{co} is the ratio between the time where the driver torque and the assist system have the same sign and the total time of the manoeuvre

$$r_{\text{co}} = \frac{1}{T} \int_0^T \text{sign}(\mathbf{T}_{\text{dr}}\mathbf{T}_c) \, dt \text{ if } \mathbf{T}_{\text{dr}}\mathbf{T}_c \geq 0. \tag{28}$$

2) Intrusiveness ratio r_{int} calculated as the ratio of the time where the driver torque and the assist system have opposite sign and the total time of the manoeuvre

$$r_{\text{int}} = \frac{1}{T} \int_0^T \text{sign}(\mathbf{T}_{\text{dr}}\mathbf{T}_c) \, dt \text{ if } \mathbf{T}_{\text{dr}}\mathbf{T}_c < 0. \tag{29}$$

3) Resistance ratio [15] r_{re} calculated as the ratio of the time where the driver torque and the assist system have opposite sign and the total time of the manoeuvre, if the driver torque is bigger than the driving assist torque

$$r_{\text{re}} = \frac{1}{T} \int_0^T \text{sign}(\mathbf{T}_{\text{dr}}\mathbf{T}_c) \, dt$$

$$\text{if } \mathbf{T}_{\text{dr}}\mathbf{T}_c < 0 \text{ and } \mathbf{T}_{\text{dr}} > \mathbf{T}_c. \tag{30}$$

4) Contradiction ratio [15] r_{cont} is the ratio of the time where the driver torque and the assist system have opposite sign and the total time of the manoeuvre, if the driver torque is smaller than the driving assist torque

$$r_{\text{cont}} = \frac{1}{T} \int_0^T \text{sign}(\mathbf{T}_{\text{dr}}\mathbf{T}_c) \, dt$$

$$\text{if } \mathbf{T}_{\text{dr}}\mathbf{T}_c < 0 \text{ and } \mathbf{T}_{\text{dr}} < \mathbf{T}_c. \tag{31}$$

5) Coherence [29], γ, defined in terms of the cosine of the angles formed by the driver and driving assist torque. It is positive if the assist system is mainly portraying a collaborative behavior during the manoeuvre.

$$\gamma = \frac{\int_0^T \mathbf{T}_{\text{dr}}\mathbf{T}_c \, dt}{\sqrt{\int_0^T \mathbf{T}_{\text{dr}}^2 \, dt \int_0^T \mathbf{T}_c^2 \, dt}}. \tag{32}$$

D. Control Authority Level

1) Level of sharing [29] T_{share} is the ratio between the assist system steering effort and the driver steering effort

$$T_{\text{share}} = \frac{se_{Tc}}{se_{Td}}. \tag{33}$$

E. Smooth Driving

1) Steering reversal rate (SRR) [30] is the number of steering wheel reversals, per minute that are larger than a gap value $\theta_{\text{sw,min}}$. To reduce high-frequency noise, the steering wheel angle and steering wheel velocity signals are filtered with a second-order Butterworth filter with cut-off frequency $f_{\text{cut}} = 0.6$ Hz. The SRR is calculated as the number of times where $|\theta_{\text{sw}}(t_1) - \theta_{\text{sw}}(t_2)| \geq \theta_{\text{sw,min}}$ for time-steps t_1, t_2 corresponding to consecutive steering wheel velocities equal to zero

$$\theta_{\text{sw,min}} = 3 \text{ deg} \tag{34}$$

$$\text{SRR} = \frac{n_{\text{change}}}{T} \cdot 60. \tag{35}$$

F. Driver Model Accuracy

1) RMSE of the predicted driver torque $T_{d,\text{pred}}$ with respect to the real driver T_d

$$\text{RMSE}_{T\text{pred}} = \sqrt{\frac{1}{N} \sum_{i=1}^{N} (T_{d,\text{pred},i} - T_{d,i})^2}. \tag{36}$$

2) Accuracy of the driver model torque prediction is

$$A(\%) = \left[1 - \frac{1}{\text{SD}(T_d)} \text{RMSE}_{T\text{pred}} \right] \cdot 100. \tag{37}$$

ACKNOWLEDGMENT

REFERENCES

[1] D. Katzourakis, N. Lazic, C. Olsson, and M. Lidberg, "Driver steering override for lane-keeping aid using computer-aided engineering," *IEEE/ASME Trans. Mechatronics*, vol. 20, no. 4, pp. 1543–1552, Aug. 2015.

[2] M. Itoh, F. Flemisch, and D. Abbink, "A hierarchical framework to analyze shared control conflicts between human and machine," *IFAC-PapersOnLine*, vol. 49, no. 19, pp. 96–101, 2016.

[3] T. A. Litman, *Autonomous Vehicle Implementation Predictions: Implications for Transport Planning*, Transportation Research Board, Washington, DC, USA, 2020.

[4] M. Mulder, D. A. Abbink, and E. Boer, "Sharing control with haptics: Seamless driver support from manual to automatic control," *Human Factors*, vol. 54, no. 5, pp. 786–798, 2012.

[5] R. Boink, M. M. van Paassen, M. Mulder, and D. A. Abbink, "Understanding and reducing conflicts between driver and haptic shared control," in *Proc. IEEE Int. Conf. Syst., Man, Cybern.*, 2014, pp. 1510–1515.

[6] D. Franklin, R. Osu, E. Burdet, M. Kawato, and T. Milner, "Adaptation to stable and unstable dynamics achieved by combined impedance control and inverse dynamics model," *J. Neuriophysiol.*, vol. 90, no. 5, pp. 3270–3282, 2003.

[7] D. A. Abbink and M. Mulder, "Neuromuscular analysis as a guideline in designing shared control," in *Proc. Adv. Haptics. IntechOpen*, pp. 499–516, 2010.

[8] C. Lv *et al.*, "Characterization of driver neuromuscular dynamics for human-automation collaboration design of automated vehicles," *IEEE/ASME Trans. Mechatronics*, vol. 23, no. 6, pp. 2558–2567, Dec. 2018.

[9] F. Mars, L. Saleh, P. Chevrel, F. Claveau, and J. Lafay, "Modeling the visual and motor control of steering with an eye to shared-control automation," in *Proc. Human Factors Ergonom. Soc. Annu. Meeting*, 2011, vol. 55, no. 1, pp. 1422–1426.

[10] M. Marcano, S. Díaz, J. Pérez, and E. Irigoyen, "A review of shared control for automated vehicles: Theory and applications," *IEEE Trans. Human-Mach. Syst.*, vol. 50, no. 6, pp. 475–491, Dec. 2020.

[11] Z. Ercan, A. Carvalho, M. Gokasan, and F. Borrelli, "Modeling, identification, and predictive control of a driver steering assistance system," *IEEE Trans. Human-Mach. Syst.*, vol. 47, no. 5, pp. 700–710, Oct. 2017.

[12] Z. Ercan, A. Carvalho, H. Tseng, and F. Borrelli, "A predictive control framework for torque-based steering assistance to improve safety in highway driving," *Veh. Syst. Dyn.*, vol. 56, no. 5, pp. 810–831, 2018.

[13] C. Guo, C. Sentouh, J. Haué, and J. Popieul, "Driver-vehicle cooperation: A hierarchical cooperative control architecture for automated driving systems," *Cognition, Technol. Work*, vol. 21, no. 4, pp. 657–670, 2019.

[14] C. Lv *et al.*, "Human-machine collaboration for automated driving using an intelligent two-phase haptic interface," *Adv. Intell. Syst.*, pp. 1–12, 2021, doi: 10.1002/aisy.202000229.

[15] L. Saleh, P. Chevrel, F. Claveau, J. F. Lafay, and F. Mars, "Shared steering control between a driver and an automation: Stability in the presence of driver behavior uncertainty," *IEEE Trans. Intell. Transp. Syst.*, vol. 14, no. 2, pp. 974–983, Jun. 2013.

[16] X. Ji, K. Yang, X. Na, C. Lv, and Y. Liu, "Shared steering torque control for lane change assistance: A stochastic game-theoretic approach," *IEEE Trans. Ind. Electron.*, vol. 66, no. 4, pp. 3093–3105, Apr. 2019.

[17] X. Na and D. J. Cole, "Game theoretic modeling of the steering interaction between a human driver and a vehicle collision avoidance controller," *IEEE Trans. Human-Mach. Syst.*, vol. 45, no. 1, pp. 25–38, Feb. 2015.

[18] S. Ko and R. Langari, "Shared control between human driver and machine based on game theoretical model predictive control framework," in *Proc. IEEE/ASME Int. Conf. Adv. Intel. Mech.*, 2020, pp. 649–654.

[19] W. Scholtens, S. Barendswaard, D. M. Pool, M. van Paassen, and D. Abbink, "A new haptic shared controller reducing steering conflicts," in *Proc. IEEE Int. Conf. Syst., Man, Cybern.*, 2018, pp. 2705–2710.

[20] T. Niu and D. Cole, "A model of driver steering control incorporating steering torque feedback and state estimation," Dept. of Eng., Univ. Cambridge, Tech. Rep. ENG-TR 005, 2020.

[21] C. J. Nash and D. J. Cole, "Identification and validation of a driver steering control model incorporating human sensory dynamics," *Veh. Syst. Dyn.*, vol. 58, no. 4, pp. 495–517, 2020.

[22] R. S. Sharp and V. Valtetsiotis, "Optimal preview car steering control," *Veh. Syst. Dyn.*, vol. 35, no. S1, pp. 101–117, 2001.

[23] J. M. Winters and L. Stark, "Muscle models: What is gained and what is lost by varying model complexity," *Biol. Cybern.*, vol. 55, no. 6, pp. 403–420, 1987.

[24] B. Shyrokau *et al.*, "The effect of steering-system linearity, simulator motion, and truck driving experience on steering of an articulated tractor-semitrailer combination," *Appl. Ergonom.*, vol. 71, pp. 17–28, 2018.

[25] S. Kolekar, W. Mugge, and D. Abbink, "Modeling intradriver steering variability based on sensorimotor control theories," *IEEE Trans. Human-Mach. Syst.*, vol. 48, no. 3, pp. 291–303, Jun. 2018.

[26] M. Damian, B. Shyrokau, A. Ocariz, and X. C. Akutain, "Torque control for more realistic hand-wheel haptics in a driving simulator," in *Proc. Driving Simul. Conf. Europe*, 2019, pp. 35–42.

[27] T. Inagaki, "Adaptive automation: Sharing and trading of control," in *Handbook of Cognitive Task Design*. Mahwah, NJ, USA: Lawrence Erlbaum Associates, 2003, pp. 147–169.

[28] B. Houska, H. Ferreau, and M. Diehl, "ACADO toolkit-an open-source framework for automatic control and dynamic optimization," *Optimal Control Appl. Methods*, vol. 32, no. 3, pp. 298–312, 2011.

[29] B. Pano, Y. Zhao, P. Chevrel, F. Claveau, and F. Mars, "Shared control based on an ecological feedforward and a driver model based feedback," in *Proc. 9th IFAC Int. Symp. Adv. Autom. Control*, 2019, pp. 385–392.

[30] G. Markkula and J. Engström, "A steering wheel reversal rate metric for assessing effects of visual and cognitive secondary task load," in *Proc. 13th ITS World Congr.*, 2006, pp. 1–12.

Andrea Michelle Rios Lazcano received the B.Eng. degree in industrial technology engineering from the Polytechnic University of Madrid, Madrid, Spain, in 2018, and the M.Sc. (*cum laude*) degree in mechanical engineering, (with specialization in vehicle engineering) from the Delft University of Technology, Delft, The Netherlands, in 2020.

She is currently a Graduate Engineer with Toyota Motor Europe, Brussels, Belgium, and she is conducting research on control algorithms for symbiotic automated driving. Her research interests include MPC, driver modeling, and vehicle dynamics.
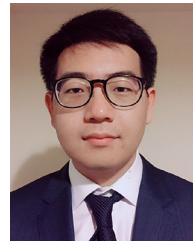
Tenghao Niu received the B.Eng. degree in mechanical engineering from the Department of Mechanical, Materials and Manufacturing Engineering, The University of Nottingham, Nottingham, U.K., in 2017. He is currently working toward the Ph.D. degree in modeling of driver-vehicle dynamics from the Driver-Vehicle Dynamics Research Group, Department of Engineering, University of Cambridge, Cambridge, U.K.

His main research interests include driver modeling, vehicle dynamics, steering torque feedback, state estimation, and optimal control.

Xabier Carrera Akutaín received the Ph.D. degree in mechanical engineering from the University of Navarra, Pamplona, Spain, in 2006.

He was with Toyota Motor Europe (TME), Brussels, Belgium, as a Senior Engineer in Vehicle Dynamics in 2009. From 2013 to 2015, he was an Expert Vehicle Dynamics with Toyota Motor Corporation, Toyota, Japan. Since 2016, he has been the Manager with the Vehicle Dynamics and Virtual Evaluation Group, TME, Belgium. His research interests include the human perception of performance metrics and driving simulator toolchain development.
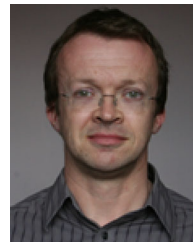
David Cole received the B.A./M.A. degree in engineering and the Ph.D. degree in vehicle dynamics from the Department of Engineering, University of Cambridge (Cambridge), Cambridge, U.K., in 1985 and 1990, respectively.

From 1990 to 1996, he undertook Postdoctoral Research in Heavy Vehicle Dynamics with Cambridge. From 1996 to 2000, he was a Lecturer with the University of Nottingham, Nottingham, U.K. In 2000, he returned to Cambridge, where he is a Reader of mechanical engineering. His main research interest includes driver–vehicle dynamics.

Dr. Cole is a Chartered Engineer and a Fellow of the Institution of Mechanical Engineers.

Barys Shyrokau received the Dipl.Eng. degree (*cum laude*) in mechanical engineering from the Belarusian National Technical University, Minsk, Belarus, in 2004, and the joint Ph.D. degree in control engineering from Nanyang Technological University, Singapore, and Technical University Munich, Munich, Germany, in 2015.

He is currently an Assistant Professor with the Section of Intelligent Vehicles, Department of Cognitive Robotics, The Delft University of Technology, Delft, The Netherlands and involved in research related to vehicle dynamics and control, motion comfort, and driving simulator technology.

Dr. Shyrokau was the Recipient of the scholarship and award of FISITA, DAAD, SINGA, ISTVS, and CADLM.